

Random Field Driven Spatial Complexity at the Mott Transition in VO₂

Shuo Liu,^{1,*} B. Phillabaum,¹ E. W. Carlson,¹ K. A. Dahmen,²
N. S. Vidhyadhiraja,³ M. M. Qazilbash,⁴ and D. N. Basov⁵

¹*Department of Physics, Purdue University, West Lafayette, IN 47907, USA*

²*Department of Physics, University of Illinois, Urbana-Champaign, IL 61801, USA*

³*Jawaharlal Nehru Centre for Advanced Scientific Research, Bangalore 560064, India*

⁴*Department of Physics, College of William and Mary, Williamsburg, VA 23187, USA*

⁵*Department of Physics, University of California-San Diego, La Jolla, CA 92093, USA*

(Dated: March 4, 2022)

We report the first application of critical cluster techniques to the Mott metal-insulator transition in vanadium dioxide. We show that the geometric properties of the metallic and insulating puddles observed by scanning near-field infrared microscopy are consistent with the system passing near criticality of the random field Ising model as temperature is varied. The resulting large barriers to equilibrium may be the source of the unusually robust hysteresis phenomena associated with the metal-insulator transition in this system.

The Mott metal-insulator transition in VO₂ has the potential to produce disruptive technologies, such as memristors, memory capacitors, ultrafast switches, and possibly even neuromorphic circuits [1]. Yet despite decades of research into the Mott metal-insulator transition in VO₂, the nature of the phase transition, and in particular the broad hysteretic behavior accompanying it, is not yet understood. The Mott metal-insulator transition has some universal features of the liquid-gas transition [2, 3]: the transition occurs through a first order phase transition line broadened by conductivity hysteresis, which terminates at a classical critical point associated with general Ising universality [2–6]. In addition, in VO₂ a percolation model has been proposed through the study of resistance avalanches [7], while in V₂O₃ the clean 3D Ising model has been implicated [2]. By applying quantitative critical cluster techniques to study the criticality, we show that a key ingredient missing from prior treatments is the prominent role of disorder, with important implications for the robust hysteresis effects associated with the metal-insulator transition.

As shown in Fig. 1, scanning near-field infrared microscopy (SNIM) on VO₂ [8] reveals the complex pattern formation associated with the transition from the low temperature insulating phase to the high temperature metallic phase. We apply recently developed cluster techniques [9] to the observed multiscale patterns of inhomogeneous local conductivity, revealing critical exponents such as the fisher exponent τ , volume fractal dimension d_v , and hull fractal dimension d_h , both for clusters and avalanches. This method has the advantage that it can access the true universality class of the phase transition, unlike methods based on macroscopic conductivity in which the exponents are affected by the contrast ratio between metallic and insulating regions [3]. Our analysis is the first to quantitatively incorporate disorder into the study of the criticality, allowing us to determine the relative importance of disorder and interactions, and identify the dominant type of disorder.

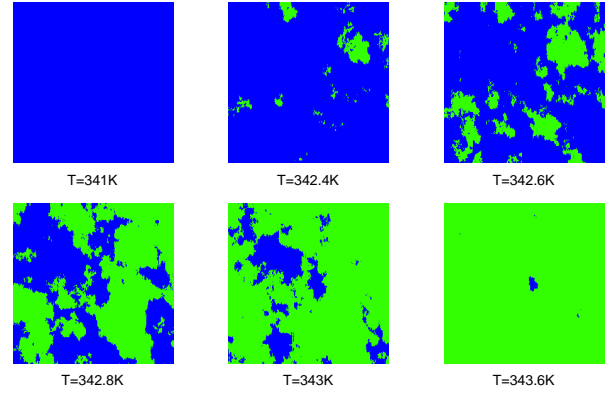


FIG. 1. Scanning Near-field Infrared Microscopy on VO₂ as temperature is increased through the Mott metal-insulator transition regime, over the same $4\mu\text{m} \times 4\mu\text{m}$ sample area. These figures are Ising-mapped from the original SNIM images in Ref. [8] with threshold scattering amplitude $a_{th} = 2.5$. The metallic regions, colored green, give higher near-field scattering amplitude, $a > a_{th}$, compared with the insulating regions with $a \leq a_{th}$, colored blue.

Near a critical point, the correlation length grows to become the dominant length scale, and it is possible to map the real physical system to a coarse-grained model with the same universal features. In the original SNIM data images [8], we assign Ising variable $\sigma = 1$ (metallic) or -1 (insulating) to each coarse-grained region [2–6]. The threshold amplitude a_{th} for identifying the metallic regions (those with scattering amplitude $a > a_{th}$) and insulating regions (with $a \leq a_{th}$) is about 2.5 [8, 10], which we use throughout this Letter. We furthermore incorporate disorder into the model:

$$H = - \sum_{\langle ij \rangle_{\parallel}}^{\infty} (J + \delta J_{ij}) \sigma_i \sigma_j - \sum_{\langle ij \rangle_{\perp}}^{L_z} (J + \delta J_{ij}) \sigma_i \sigma_j - \sum_i (h + h_i) \sigma_i, \quad (1)$$

where the sum runs over the coarse-grained regions (sites) consisting of a cubic lattice, chosen with spacing at least as small as the resolution of the images to be studied. The tendency for neighboring regions to be of like character is modeled as a nearest neighbor ferromagnetic interaction $J > 0$. Because the data considered is that of a thin film, the sum over Ising variables in the plane of the film (denoted by \parallel) extends to infinity, but the sum over Ising variables perpendicular to the film surface (denoted by \perp) is finite, confined by the film thickness L_z . Depending on the size of the correlation volume compared to the size of the system, the sample may display two-dimensional (2D) or three-dimensional (3D) critical behavior near criticality.

At the order parameter level, there are two broad classes of disorder: local energy density disorder (which we incorporate as random bond disorder), and random field disorder [11]. Random bond disorder is included through the term δJ_{ij} , and h_i represents random field disorder, which is chosen from a gaussian probability distribution centered about zero, with variance R . R is often called the disorder parameter or just disorder. The field h represents a generalized external field which couples with the local Ising variables. Figure 2 shows the schematic phase diagrams associated with this general Ising model of Eqn. 1, encompassing several universality classes both in 2D and 3D. Note that random field disorder is always relevant in the renormalization group sense, and in fact if both random bond and random field disorder are present, the associated stable fixed points are those of the random field disorder.

Using our mapping to Ising variables (Fig. 1), we track the geometric clusters, defined as connected sets of nearest neighbor sites (pixels) with the same color. We then use the statistics of the sizes and shapes of these geometric clusters to identify the cause of the complex pattern formation. In comparing the spatial complexity revealed in the SNIM data to theory, there are 7 fixed points to consider, as shown in Fig. 2. In the two-dimensional case, these consist of the clean Ising model (C-2D, *i.e.* in the absence of any material disorder), uncorrelated percolation (P-2D), and the random field Ising model (RF-2D). Note that random bond disorder is irrelevant in the renormalization group sense in 2D, and the phase transition is therefore governed by clean Ising model exponents set by the C-2D fixed point. Although the RF-2D fixed point is unstable, its critical behavior can be observed for weak enough finite disorder. In the three-dimensional case, the possible fixed points are the clean Ising model (C-3D), uncorrelated percolation (P-3D), the random bond Ising model (RB-3D), and the random field Ising model (RF-3D). For the exponents extraction, in order to reduce noise due to the finite field of view (FOV), we apply the logarithmic binning method throughout this Letter, which is a standard technique for analyzing power law behavior [12]. The value of critical exponents are obtained

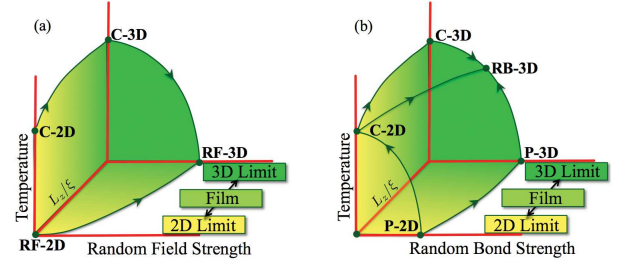


FIG. 2. Schematic equilibrium phase diagrams and fixed points of Eqn. 1. Two classes of disorder: (a) Random field disorder (with or without random bond disorder); (b) Random bond disorder in the absence of random field disorder. Solid regions denote the ordered phase, from 2D (yellow region, applicable when the correlation length $\xi \gg L_z$) to 3D (green region, applicable for ξ large but less than L_z). Solid green lines represent continuous phase transitions. The green arrow(flow) on each phase transition line points to the solid green circle representing the fixed point controlling the long distance (universal) behavior of that phase transition.

by taking the discrete logarithmic derivative (DLD) [13].

From the SNIM images, we extract three critical exponents, which are the Fisher exponent τ , the volume fractal dimension d_v , and the hull fractal dimension d_h , as entailed by the self-similarity of the geometric clusters near certain critical points. τ characterizes the cluster-size distribution $D(s)$, which is the histogram of cluster sizes s , and scales as $D(s) \propto s^{-\tau}$. d_v and d_h characterize the fractal nature of cluster sizes s and hulls h . For the cluster sizes we have $s \propto R_s^{d_v}$, where R_s is the radius of gyration of the cluster [14]. For the cluster surfaces, we have $h \propto R_h^{d_h}$. R_h here refers to the radius of gyration of *all* the sites enclosed by the hull, including any sub-clusters inside. Throughout this letter, we analyze the power law behaviors using only the internal clusters, *i.e.*, clusters which do not intersect the boundary of the FOV, in order to mitigate finite FOV effect to the extraction of exponents. Although from our analysis d_v and d_h do not appear to be affected by this effect, estimates of τ in a finite FOV are always skewed to lower values because of a pronounced bump in the scaling function of the cluster size distribution [10, 15, 16]. Within a cutoff in the decades of scaling, $D(s)$ of internal clusters would share the same power law as the full system [16], therefore τ could be extracted more accurately.

Figure 3 shows the extraction of τ , d_v , and d_h by applying our cluster techniques to the finite size SNIM image data through the Mott transition using internal clusters. The main panels show explicitly the power law fits of these critical cluster exponents at three intermediate temperatures (which have enough clusters for good statistics) with threshold scattering amplitude $a_{th} = 2.5$. For τ , two decades of scaling are evident, and the remaining points fall off the scaling regime due to the use of internal clusters [16]; and for the fractal dimensions, with the first

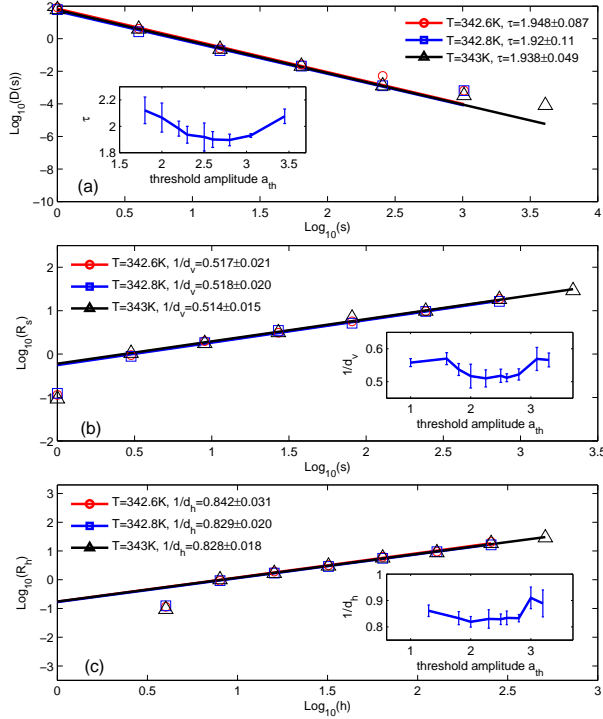


FIG. 3. Power law fits of internal clusters from the VO₂ SNIM imaging datasets with threshold scattering amplitude $a_{th} = 2.5$ for (a) $D(s) \propto s^{-\tau}$, (b) $R_s \propto s^{1/d_v}$, and (c) $R_h \propto h^{1/d_h}$, at three intermediate temperatures $T = 342.6K$, $T = 342.8K$, and $T = 343K$. The insets show τ , $1/d_v$, and $1/d_h$ (with error bars) extracted using the same method as a function of a_{th} at $T=342.8K$.

bin (which contains $s = 1$ clusters) excluded [10], robust power law scaling extends over multiple decades, encompassing the entire FOV. The robust power law behaviors as well as the fact that the values of the cluster exponents are the same within error bars for different intermediate temperatures corroborates the idea that the system is near some critical end point of the Mott transition. The insets of Fig. 3 show our extracted τ , d_v , and d_h using different a_{th} at the representative temperature $T = 342.8K$ which is closest to criticality, and within error bars these critical exponents are robust against changes in threshold amplitude within a broad stable region around $a_{th} = 2.5$, consistent with that given by the definition in the experiment paper [8, 10]. This independence of results with respect to microscopic details also reflects universal behavior near criticality. Using $a_{th} = 2.5$ and $T=342.8K$ as representative conditions, we have $\tau = 1.92 \pm 0.11$, $d_v = 1.93 \pm 0.07$, and $d_h = 1.21 \pm 0.03$ for the spatially complex clusters near the critical end point of the Mott transition in VO₂.

Before comparing the numerical values of the critical exponents revealed by our analysis of the data to the known theoretical values of each fixed point, the C-3D and RB-3D fixed points can be ruled out *a priori*. Since

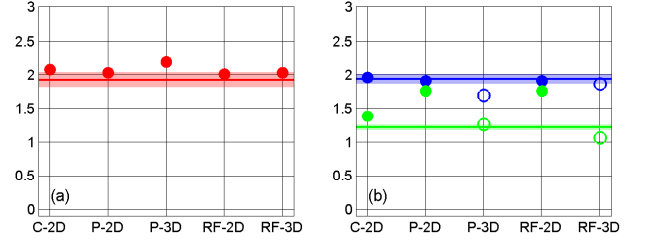


FIG. 4. Exponent comparison charts. (a) Critical exponent τ . (b) Critical exponents d_v (blue) and d_h (green). The horizontal lines are our extracted exponents from the SNIM images, with the shaded regions being their error bars. The circles represent theoretical values [9, 10] for the fixed points of Eqn. 1. When comparing with 3D models, we have to use the effective values of d_v^* and d_h^* corresponding to taking 2D cross sections of the clusters embedded in 3D, *i.e.* $d_v^* = 2d_v/3$ and $d_h^* = d_h/2$ [9, 10]. These effective values are represented by the open circles.

geometric clusters are not fractal at these two fixed points [17–19], they cannot be the cause of the robust power law behavior observed in Figs. 3(b) and 3(c). Five fixed points remain to be considered (C-2D, RF-2D, RF-3D, P-2D, and P-3D), and the geometric clusters do exhibit a fractal nature at these fixed points [13, 14, 17, 20]. In the slab geometry considered here (and also for layered materials), it is also necessary to consider possible dimensional crossovers. Within this set of candidate fixed points, there are two possible dimensional crossovers. In the presence of random field disorder, the dimensional crossover is between RF-2D and RF-3D. (For a slab geometry, exponents will drift from the 3D fixed point toward the associated 2D fixed point, once the correlation length in the c-axis direction begins to exceed the slab thickness.) The other possible dimensional crossover is between C-2D and the 3D percolation points $T_p < T_c$ in the clean and random bond Ising models. Although the exponents we require have not been explicitly reported in the literature, the expectation in the literature is that the exponents should follow those of uncorrelated percolation, P-3D [19, 21, 22].

As shown in Fig. 4, the values of τ and d_v resulting from our analysis of the data are fairly close to all fixed points other than P-3D. Therefore, uncorrelated 3D percolation can be ruled out as an origin of the power law behavior of the statistics and geometry of the metal and insulator islands. Note, however, that the theoretical values of the remaining four fixed points are all fairly close in value for these two exponents, making it hard to distinguish among the remaining fixed points using only these two measures. On the other hand, d_h varies significantly for the various fixed points. We see immediately from the comparison chart that the theoretical values of d_h at P-2D and RF-2D are inconsistent with the data. Whereas the closest match for this measure is P-3D, that is incon-

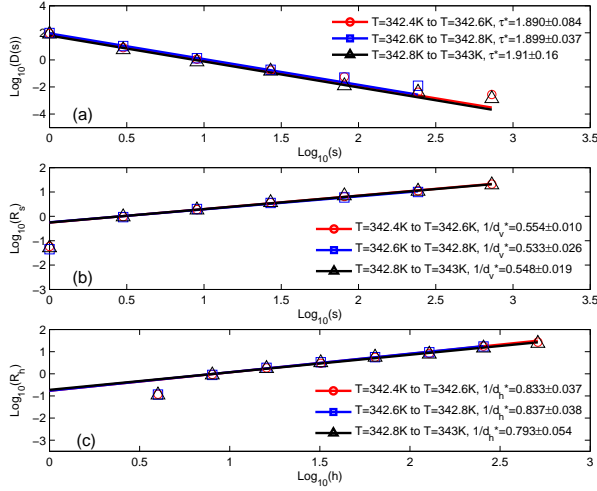


FIG. 5. Power law fits of internal avalanches from the VO₂ SNIM imaging datasets with threshold scattering amplitude $a_{th} = 2.5$ for (a) $D(s) \propto s^{-\tau^*}$, (b) $R_s \propto s^{1/d_v^*}$, and (c) $R_h \propto h^{1/d_h^*}$, at three intermediate intervals with $\Delta T = 0.2K$ through the Mott transition

sistent with the other two critical exponents, and must remain ruled out.

Only two candidate fixed points remain (C-2D and RF-3D), but in Fig. 4(b), both show about a 13% discrepancy between the data and the theoretical model for the value of d_h , which is significantly larger than the typical error of about 3% of the exponents extracted from the data. We turn then to the possibility of dimensional crossovers. In the case of the clean or random bond Ising model, power law behavior of geometric clusters will drift from P-3D to C-2D as larger length scales are observed. However, the value of d_v is much closer to C-2D than to P-3D, consistent with the geometric clusters being near their 2D limit, whereas the value of d_h is much closer to P-3D than to C-2D, which would indicate that the geometric clusters are near their 3D limit. This inconsistency strongly argues against the P-3D to C-2D dimensional crossover as the origin of the power law behavior.

The other candidate dimensional crossover is from RF-3D to RF-2D. The exponent comparisons show no inconsistency with this explanation, since within error bars τ and d_v match the whole RF-2D to RF-3D crossover regime, and d_h is also consistent with this dimensional crossover. Therefore, the random field Ising universality class best describes the critical behavior of the Mott transition in the VO₂ thin film, revealing the key role played by disorder effects in these systems. Observations at longer length scales can be used to test this hypothesis: if our identification is correct, then the values of all exponents should drift toward RF-2D with larger fields of view in a film geometry such as the present one.

In order to further test whether the spatial complex-

ity is driven by random field effects, we also analyze the avalanches which, in the context of the VO₂ experiment, are defined as the difference between Ising maps between two neighboring temperatures. We study the critical avalanche exponents arising from the self-similarity of avalanches and are directly extractable from the experimental image datasets. Figure 5 shows the power law fits of the internal avalanches with threshold $a_{th} = 2.5$ for the data-extracted τ^* , d_v^* , and d_h^* , using the same techniques as for the clusters in Fig. 3. The star symbol is used to denote that these exponents are for avalanches. Similar to their cluster counterparts, the cut-off for internal avalanche scaling for τ^* is about 1.5 to 2 decades of scaling, and d_v^* and d_h^* show multiple decades of power law scaling behavior. For different intervals, the extracted critical avalanche exponents are consistent with each other within error bars. This data-extracted robust universal power law scaling of avalanches provides further evidence that the random field universality is underlying the complex pattern formation at the Mott transition in the VO₂ thin film, since non-trivial scaling behavior of avalanches is characteristic of random field physics.

Since the avalanches are taken from the finite interval between scanned images, the data-extracted τ^* in our context characterizes the scaling of the field integrated avalanche size distribution $D_{int}(s)$ near criticality. The corresponding exponent is reported to be 2.03 ± 0.03 for RF-3D [15, 23, 24] and 1.3 ± 0.1 [25] for RF-2D, and the corresponding data-extracted one from Fig. 5(a) lies in between, consistent with the conclusion of a dimensional crossover from RF-3D to RF-2D. With d_v^* and d_h^* only reported for RF-3D [24], our data-extracted fractal dimensions Fig. 5(b) and (c) could not be directly compared with the theoretical ones. However, by comparison with Fig. 3(b) and (c), within error bars d_v and d_h extracted from avalanches have the same values as those from clusters, consistent with Ref. [24], which show that clusters and avalanches have the same exponents in random field Ising model (RFIM).

The dominance of random field disorder is quite reasonable in a real physical system, arising from defects and impurities in the crystal structure; randomness in grain size, orientation, and boundary structure; and imperfections in the substrate. In particular, it has been shown that the temperature at which grains transition depends on grain size [26]. In addition, we have previously shown that metallicity nucleates first near the grain boundaries (see Fig. 6 of Ref [27]). Since physical temperature maps to effective field in our model, these effects map to random field disorder in the model. (See SI for a more thorough discussion.) One prediction of this line of reasoning is that grain size, since it affects the random field strength in the model, is expected to correlate with the hysteresis width.

Several other characteristics of the data serve to corroborate the random field hypothesis. For example, as

the Mott transition proceeds, metallic puddle formation occurs via nucleation and not exclusively by front propagation [28], as can be seen in Fig. 1. In addition, as temperature increases through the transition (analogous here to sweeping the generalized field h of Eqn. 1), domains change from $\sigma = -1$ to $\sigma = +1$, but never revert. This no-passing rule is consistent with the random field universality class [24, 29, 30], indicating that the effects of quenched disorder dominate over thermal fluctuations. The dominance of quenched disorder over thermal effects is further corroborated by the reproducibility of the SNIM images, in that repeated near-field scans in the insulator-to-metal transition regime over the same sample area and at a fixed temperature show nearly identical patterns of metallic puddles in the insulating host [8, 31].

Finally, perhaps the most tell-tale sign of random field behavior in the data is the large width of the hysteresis in temperature, about $7.5K$ for temperature sweeps taking several minutes in a thin film [31, 32]. The extreme critical slowing down of the random field case means that barriers to equilibration grow much more severely as criticality is approached than the usual “critical slowing down” would predict. Hysteresis typically becomes long-lived near the critical endpoint of a first order phase transition, with the relaxation time t_{rel} diverging as a power law near the critical endpoint [33], $t_{rel} \propto \xi^z \propto |g - g_c|^{-\nu z}$, where g represents the relevant variable, whether temperature T or disorder strength R . ξ is the correlation length, ν is the exponent of the correlation length, and z is the dynamical exponent. Rather than a mere power law, barriers to equilibration grow exponentially near the RFIM critical endpoint [34], $t_{rel}^{RFIM} \propto \exp[\xi^\theta] \propto \exp[1/|g - g_c|^{\nu\theta}]$, where θ is the “violation of hyperscaling” exponent. These exponentially large barriers to equilibration are consistent with the large width of hysteresis loops evident in this Mott metal-insulator transition. In addition, the large critical region typically associated with RFIM physics [15] is consistent with the wide range of parameters over which the broad hysteresis is observed.

In conclusion, by applying newly developed cluster techniques to SNIM data on VO_2 , we have shown using three different critical exponents that the critical endpoint of the Mott transition is in the universality class of the random field Ising model. This finding reveals a delicate interplay between interaction and disorder in these systems. The random field Ising universality class has also recently been shown to account for the spatial structure of the locally oriented domains observed via scanning tunneling microscopy on cuprate superconductors [9, 35]. This further emphasizes the important role played by disorder in strongly correlated electron systems, and indicates that there may be universality to the spatial complexity [36, 37] observed in a wide variety of strongly correlated electron systems. The cluster

techniques employed here can readily be applied to 2D images in the context of other materials and microscopy techniques for the study of critical behavior.

We thank H. Aubin, J. Honig, and A. Zimmers for helpful conversations. S.L., B.P., and E.W.C. acknowledge support from NSF Grant No. DMR 11-06187. E.W.C. acknowledges receipt of an APS-IUSSTF Professorship Award, and thanks JNCASR for hospitality. K.A.D. acknowledges support from NSF Grant No. DMR 10-05209 and NSF Grant No. DMS 10-69224. N.S.V. acknowledges IUSSTF, JNCASR and Purdue University for funding the visitor exchange program. M.M.Q. acknowledges support from NSF Grant No. DMR 12-55156. D.N.B. acknowledges support from DOE-BES.

* liu305@purdue.edu

- [1] Z. Yang, C. Ko, and S. Ramanathan, *Annu. Rev. Mater. Res.* **41**, 337 (2011).
- [2] P. Limelette, A. Georges, D. Jérôme, P. Wzietek, P. Metcalf, and J. M. Honig, *Science* **302**, 89 (2003).
- [3] S. Papanikolaou, R. M. Fernandes, E. Fradkin, P. W. Phillips, J. Schmalian, and R. Sknepnek, *Phys. Rev. Lett.* **100**, 026408 (2008).
- [4] F. Kagawa, K. Miyagawa, and K. Kanoda, *Nature* **436**, 534 (2005).
- [5] C. Castellani, C. Di Castro, D. Feinberg, and J. Ranninger, *Phys. Rev. Lett.* **43**, 1957 (1979).
- [6] G. Kotliar, E. Lange, and M. J. Rozenberg, *Phys. Rev. Lett.* **84**, 5180 (2000).
- [7] A. Sharoni, J. G. Ramírez, and I. K. Schuller, *Phys. Rev. Lett.* **101**, 026404 (2008).
- [8] M. M. Qazilbash, M. Brehm, B.-G. Chae, P.-C. Ho, G. O. Andreev, B.-J. Kim, S. J. Yun, A. V. Balatsky, M. B. Maple, F. Keilmann, H.-T. Kim, and D. N. Basov, *Science* **318**, 1750 (2007).
- [9] B. Phillabaum, E. W. Carlson, and K. A. Dahmen, *Nat. Commun.* **3**, 915 (2012).
- [10] See Supplemental Material at [URL will be inserted by publisher] for details.
- [11] J. Cardy, *Scaling and Renormalization in Statistical Physics* (Cambridge University Press, Cambridge, 1996).
- [12] M. E. J. Newman, *Contemporary Physics* **46**, 323 (2005).
- [13] A. A. Middleton and D. S. Fisher, *Phys. Rev. B* **65**, 134411 (2002).
- [14] D. Stauffer and A. Aharony, *Introduction to Percolation Theory* (Taylor & Francis, London, 1992).
- [15] O. Perković, K. Dahmen, and J. P. Sethna, *Phys. Rev. Lett.* **75**, 4528 (1995).
- [16] Y.-J. Chen, S. Papanikolaou, J. P. Sethna, S. Zapperi, and G. Durin, *Phys. Rev. E* **84**, 061103 (2011).
- [17] A. Coniglio, C. R. Nappi, F. Peruggi, and L. Russo, *J. Phys. A* **10**, 205 (1977).
- [18] P. E. Berche, C. Chatelain, B. Berche, and W. Janke, *Eur. Phys. J. B* **38**, 463 (2004).
- [19] V. S. Dotsenko, M. Picco, P. Windey, G. Harris, E. Martinec, and E. Marinari, *Nucl. Phys. B* **448**, 577 (1995).
- [20] E. T. Seppälä, V. Petäjä, and M. J. Alava, *Phys. Rev. E* **58**, R5217 (1998).

- [21] J. L. Cambier and M. Nauenberg, Phys. Rev. B **34**, 8071 (1986).
- [22] D. A. Huse and S. Leibler, J. Phys. France **49**, 605 (1988).
- [23] Y. Liu and K. A. Dahmen, Phys. Rev. E **79**, 061124 (2009).
- [24] Y. Liu and K. A. Dahmen, Europhys. Lett. **86**, 56003 (2009).
- [25] C. Frontera and E. Vives, Phys. Rev. E **62**, 7470 (2000).
- [26] E. U. Donev, R. Lopez, L. C. Feldman, and R. F. Haglund, Nano Letters **9**, 702 (2009).
- [27] A. Frenzel, M. M. Qazilbash, M. Brehm, B.-G. Chae, B.-J. Kim, H.-T. Kim, A. V. Balatsky, F. Keilmann, and D. N. Basov, Phys. Rev. B **80**, 115115 (2009).
- [28] J. P. Sethna, K. A. Dahmen, and C. R. Myers, Nature **410**, 242 (2001).
- [29] J. P. Sethna, K. Dahmen, S. Kartha, J. A. Krumhansl, B. W. Roberts, and J. D. Shore, Phys. Rev. Lett. **70**, 3347 (1993).
- [30] A. A. Middleton, Phys. Rev. Lett. **68**, 670 (1992).
- [31] M. M. Qazilbash, M. Brehm, G. O. Andreev, A. Frenzel, P.-C. Ho, B.-G. Chae, B.-J. Kim, S. J. Yun, H.-T. Kim, A. V. Balatsky, O. G. Shpyrko, M. B. Maple, F. Keilmann, and D. N. Basov, Phys. Rev. B **79**, 075107 (2009).
- [32] S. Kumar, M. D. Pickett, J. P. Strachan, G. Gibson, Y. Nishi, and R. S. Williams, Adv. Mater. **25**, 6128 (2013).
- [33] B. K., J. Phys. Colloques **41**, C4 (1980).
- [34] D. S. Fisher, Phys. Rev. Lett. **56**, 416 (1986).
- [35] Y. Kohsaka, C. Taylor, K. Fujita, A. Schmidt, C. Lupien, T. Hanaguri, M. Azuma, M. Takano, H. Eisaki, H. Takagi, S. Uchida, and J. C. Davis, Science **315**, 1380 (2007).
- [36] E. Dagotto, Science **309**, 257 (2005).
- [37] A. Moreo, M. Mayr, A. Feiguin, S. Yunoki, and E. Dagotto, Phys. Rev. Lett. **84**, 5568 (2000).